CTBTO PREPARATORY COMMISSION

SnT 2019
CTBT: SCIENCE AND TECHNOLOGY CONFERENCE

Long-range ocean sound propagation effects related to the search for the Argentine submarine ARA San Juan

Peter L. Nielsen, IDC, Peter.Nielsen@ctbto.org, Mario Zampolli, IMS, Mario.Zampolli@ctbto.org,
Ronan Le Bras, IDC, RonanLeBras@ctbto.org, Georgios Haralabus, IMS, Georgios.Haralabus@ctbto.org

Poster No.
T1.3-P4

Introduction

On November 15th , 2017, the CTBT IMS hydrophone stations HA10 and HA04 detected a hydroacoustic anomaly of unknown origin. Localization of the event by associating the recorded signals at the two hydrophone stations revealed a location close to the last known position of the missing Argentine submarine ARA San Juan [1] (Fig. 1).

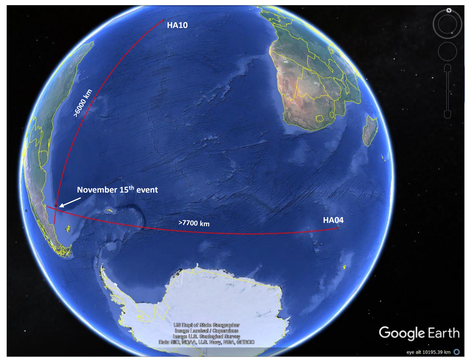

Figure 1. Location of the hydrophone stations HA10 (Ascension Island in the Atlantic Ocean) and HA04 (Crozet Islands in the Southern Indian Ocean) and the geodesic propagation paths (red lines) from the stations to the estimated event location where the paths intersect.

The localization of the event was performed by analysts after manually associating the recorded signals at the hydrophone stations as the CTBT IDC automatic processing did not form the event automatically due to erroneous phase identification at HA04. In depth analysis of the time series clearly indicates that the recorded signals exhibit very different characteristics that possibly can prevent associations although they originate from the same event. The differences in the signals recorded at the two stations are mainly related to high attenuation of the higher-frequency components and a strong channel time dispersion of the signal recorded at HA04 compared to the recording at HA10, see Fig. 2.

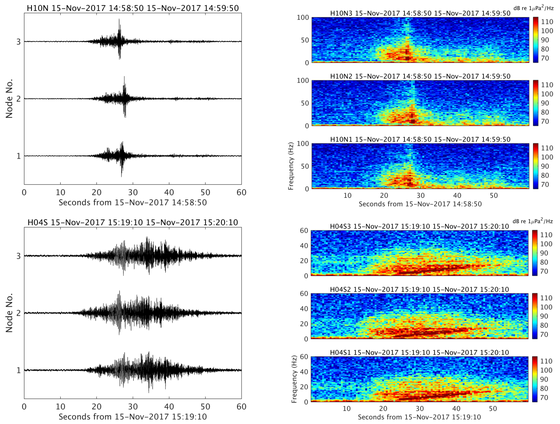

Figure 2. Normalized time-series recorded on each of the three nodes at triplets H10N (upper left) and H04S (lower left) from the November 15th event. The calibrated spectrograms for H10N and H04S are shown in the upper right and left panels, respectively.

Prediction of sound propagation in the oceans that includes spatio-temporal variations in the underwater environment can provide insight about the impact of different paths on the sound propagation from the source to the receiver locations. These predictions can assist in signal associations in cases where the recorded signals do not originate from the same source. An interpretation of the recorded signals on November 15th, 2017, at hydrophone stations HA10 and HA04 is performed by applying a numerical underwater sound propagation algorithm.

The Underwater Environment

Computation of underwater sound propagation requires reliable inputs of underwater environmental parameters. The water-column sound-speed profile and bathymetry are extracted from oceanographic databases [2,3] and interpolated along geodesic paths from the Northern hydrophone triplet H10N at HA10 and the Southern triplet H04S at HA04 to the November 15th event location. The seabed properties are assumed constant with sandy-like properties. A vertical slice of the underwater environmental scenario from H10N and H04S towards the November 15th event location is shown in Fig. 3 upper and lower panel, respectively.

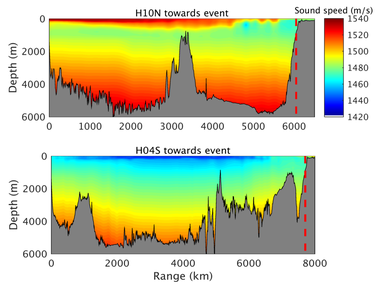

Figure 3. Vertical slice of the underwater environmental scenario along geodesic paths from the hydrophone triplets H10N (upper panel) and H04S (lower panel), respectively, and November 15th event location. The vertical dashed red line indicates the event location.

A clear duct, i.e., the Sound Fixing and Ranging channel (SOFAR), in the sound speed at H10N (upper panel at range 0 km) appears at a depth of around 1000 m close to the depth of the hydrophones. This duct tends to become shallower towards the November 15th event location at a range of approximately 6050 km. The sound speed along the 7710 km path from H04S to the November 15th event location (lower panel) represents a typical upward refracting polar profile with slightly warmer water closer to the triplet and event location. The depth of the H04S triplet hydrophones at 0 km range is 550 m. Extracting ice-sheet coverage for the period from a database [4] reveals that the sound along the path between H04S and event most likely travels under and possibly in the Antarctic ice-sheet [1] (Fig. 4).

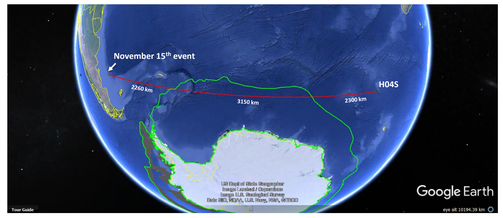

Figure 4. Geodesic path (red line) from the November 15th event to the H04S triplet that intersects with the Antarctic ice-sheet cover (green curve) for that month.

The sound is upward refracting along this geodesic path and will interact with both the sea surface and the ice sheet. High attenuation at higher acoustic frequencies is expected when the sound interacts with the ice sheet (Fig. 2). The ice sheet has elastic properties with typical values of compressional speed 3564 m/s, shear speed 1705 m/s, density 0.9 g/cm^3, compressional wave attenuation 0.5 dB/λ (λ is the acoustic wave length) and shear wave attenuation 1.0 dB/λ [5,6]. The thickness of the ice sheet is assumed to be 2-10 m. However, in the acoustic propagation computations shown here the ice-sheet is modelled as a fluid (no shear waves supported).

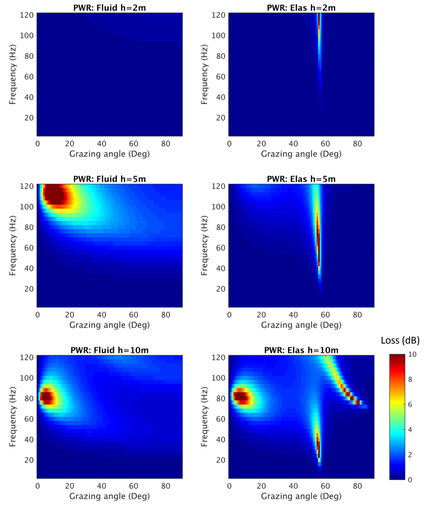

Figure 5. Comparison between plane wave reflection loss obtained with the effective fluid model expedient for the ice layer (left panels) and the full elastic ice model (right panels) as a function of frequency and grazing angle for thicknesses of 2, 5 and 10 m.

As an expedient to circumvent this limitation, effective fluid ice-sheet properties to represent a compressional wave reflection loss at the flat fluid ice-water boundary similar to the one found at an elastic ice-water boundary [7] were determined. This was obtained by an exhaustive search for compressional speed and attenuation for the fluid ice sheet that minimized a least-mean-square between the fluid and elastic frequency and grazing-angle dependent plane wave reflection loss [8] for ice sheets of 2, 5 and 10-m thickness. It was necessary to reduce the shear speed to 1442 m/s for the elastic ice sheet to obtain a high reflection loss at acoustic frequencies above 40 Hz and grazing angles below 20° as observed in the data (Fig. 2). The comparison between fluid (left panels) and elastic (right panels) reflection losses as a function of frequency and grazing angle for thicknesses of 2, 5 and 10 m is shown in Fig. 5 using the optimum parameters for the fluid ice sheet. The best match between the fluid and elastic ice-sheet reflection loss was for a 10-m thick ice layer with a compressional wave speed of 1320 m/s and compressional wave attenuation of 1.8 dB/λ (lower panel in Fig. 5).

Sound propagation modelling

Sound propagation modelling from the November 15th event location to the hydrophone triplets H10N and H04S was performed by using a modified version of the two-dimensional Parabolic Equation model RAM [9]. The propagation model was modified to include a partially covered sea surface with a fluid ice layer. The extracted environmental parameters from the oceanographic databases (Fig. 3) were used as input to RAM computing the complex acoustic pressure as a function of range and depth along the two geodesic paths between event and triplet locations (Fig. 1). Note that reciprocity is applied, i.e., the point source in the modelling is located at the known positions of the hydrophones providing the complex pressure at locations on a predefined computational grid in range and depth. Full time series were constructed at the computation grid points along the propagation paths by Fourier synthesis assuming a band-limited (1-100 Hz) sync function as the source signal. The source characteristic of the November 15th event was not included as it is unknown. The computations were performed for a maximum time window of 64 s to prevent wrap around of the received signal in the time window.

The results of the sound propagation computation along the geodesic path from the H10N triplet to the event location at a range of 6050 km from the triplet are shown in Fig. 6. The left panel in Fig. 6 shows the received time series computed at selected depths in the ocean at the event location, and the middle panel is a spectrogram of these synthetic time series at an event depth of 395 m. The right panel is the calibrated spectrogram of the data. The computed time series and spectrogram are typical for deep water propagation with the acoustic source in the SOFAR channel. Low amplitude arrivals from paths propagating along steeper paths relative to the horizontal arrive first because these arrivals travel in water with high sound speed. The high amplitude late arrivals are confined to the SOFAR channel and propagate almost horizontally at depths with low sound speed. These modelling results compare well to the data (Fig. 6 right panel).

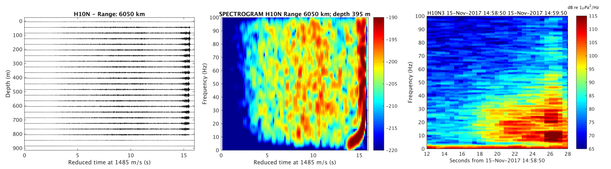

Figure 6. Left panel shows the computed time series at the November 15th event location 6050 km from the H10N triplet as a function of event depth. The middle panel is the spectrogram of the time series at an event depth of 395 m and range 6050 km from the triplet. The right panel is the calibrated spectrogram of the data.

Similar calculations of the sound propagation along the geodetic path from the H04S triplet to the November 15th event at a range of 7710 km are shown in Fig. 7. The ice sheet effect is not included in the calculations. Note the widening in computed signal time window from 16 s in Fig. 6 to 64 s in Fig. 7. The signal amplitude is clearly more evenly spread over a larger time window (Fig. 7 left panel) compared to the signal in Fig. 6 left panel. The computed signal is significantly more dispersed for the H04S-to-event path than the H10N-to-event path as observed in the data (Fig. 2). This increased time dispersion is caused by the deep-water upward refracting sound-speed profile with both shallow and steep vertically refracted sound paths interacting with the sea surface.

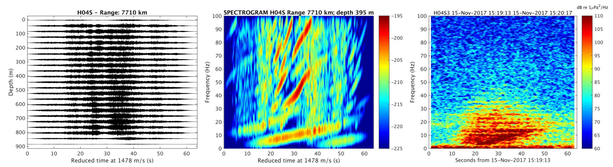

Figure 7. Left panel shows the computed time series at the November 15th event location 7710 km from the H04S triplet as a function of event depth. The middle panel is the spectrogram of the time series at an event depth of 395 m and range 7710 km from the triplet. The computation does not include an ice sheet. The right panel is the calibrated spectrogram of the data.

The synthetic spectrogram (Fig. 7 middle panel) at an event depth of 395 m reveals nearly linear dependent time-frequency bands of high signal amplitude. The slope of these striations appears to increase at higher frequencies for this particular event range and depth combination. The strong striation in the synthetic results at frequencies below 25 Hz (Fig. 7 middle panel) is also observed in the data (Fig. 7 right panel)

In the successive step, The fluid ice sheet was introduced in the propagation modelling as an abrupt change in the upper 10 m of the water-column properties at a range of 2300 km from the H04S triplet. The 10-m thick fluid ice sheet with constant properties continues out to a range of 5400 km from H4S.

At this range, the shallowest part of the water-column was abruptly changed back to simulate a pressure release sea surface and kept out to the maximum propagation range at the November 15th event location. The full thickness of the ice sheet extends into the water column and the upper surface of the sheet is at zero depth at the sea surface. The results from the sound propagation computation in a format similar to Fig. 7 , but including the 10-m thick fluid ice sheet, are shown in Fig. 8.

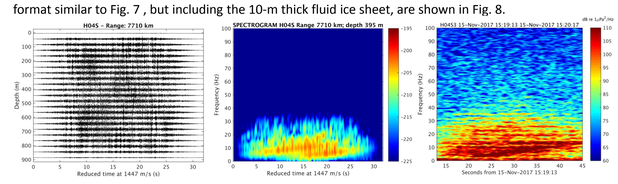

Figure 8. Left panel shows the computed time series at the November 15th event location 7710 km from the H04S triplet as a function of event depth. The middle panel is the spectrogram of the time series at an event depth of 395 m and range 7710 km from the triplet. The computation includes a 10-m thick ice sheet. The right panel is the calibrated spectrogram of the data.

The sound propagation modelling including a fluid ice sheet clearly introduces a strong low-pass filtering effect (Fig. 7 middle panel) as observed in the data (Fig. 7 right panel). The dispersion of the signal is slightly reduced and the low-frequency striation is preserved, although the striation is more diffused compared to the modelling without an ice sheet. The modeling results compare to the data fairly well when key physical properties of the underwater environment are included in the model.

The striations in the modelled spectrogram depend on the event depth as illustrated in Fig. 8. The spectrogram in Fig. 8 left panel is calculated for an event depth of 45 m, middle panel an event depth of 395 m and the right panel an event depth of 795 m. The spectrogram for the shallowest and deepest event depth is approximately 45 m from the sea surface and seabed, respectively.

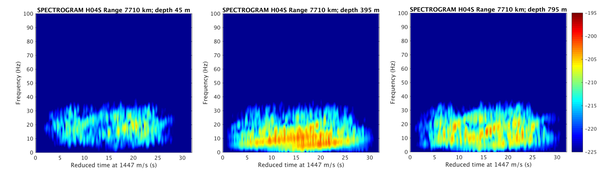

Figure 9. Computed spectrograms at the November 15th event location 7710 km from the H04S triplet at an event depth of 45 m (left panel, 395 m (middle panel) and 795 m (right panel), respectively. The striations are more diffuse as the event depth is closer to the sea surface and seabed.

The event depth at 395 m appears to be more similar to the observations than the event depths located close to the ocean boundaries. This indicates that the event most likely has happened distant from the ocean boundaries.

Conclusions

Recordings of hydroacoustic signals related to the search of the missing Argentine submarine ARA San Juan propagating long distances in the Southern Atlantic and South Indian Ocean originating from the same event reveal very different characteristics. These differences made it difficult to automatically associate the signals to that same event. The different signal characteristics are caused by very different underwater environments between source and receiver through which the signals propagate. The most significant differences in this sense are the water-column sound-speed profiles and possible under ice propagation near Antarctica. Numerical sound propagation modelling of the recorded signals using a high-fidelity two-dimensional Parabolic Equation model with realistic input parameters extracted from oceanographic databases provides a fairly good agreement with the observations and helps in the interpretation of the differences observed between the signals received at the two hydroacoustic stations. This demonstrates the potential of introducing high-fidelity underwater sound propagation modelling in automatic processing algorithms to detect, localize and classify recorded signals when these signals have very different characteristics caused by differences in the underwater environments between source and receivers.

References

[1] Peter L. Nielsen, Mario Zampolli, Ronan Le Bras, Pierrick Mialle, Paulina Bittner, Alexander Poplavskiy, Mikhail Rozhkov, Georgios Haralabus, Elena Tomuta, Randy Bell, and Patrick Grenard, “Analysis of hydro-acoustic and seismic signals originating from a source in the vicinity of the last known location of the Argentinian submarine ARA San Juan”, EGU2018-18559 PICO presentation European Geosciences Union General Assembly, Vienna, Austria, 2018.
[2] Generated using E.U. Copernicus Marine Service Information. http://marine.copernicus.eu/services-portfolio/access-to-products/
[3] The GEBCO Digital Atlas published by the British Oceanographic Data Centre on behalf of IOC and IHO, 2003. https://www.gebco.net/data_and_products/gridded_bathymetry_data/
[4] Seasonal Antarctic ice-sheet for November 15th from U.S. National Ice Center / Naval Ice Center. http://www.natice.noaa.gov/products/daily_products.html
[5] Kevin L. Williams et al. Noise Background Levels and Noise Event Tracking/Characterization Under the Arctic Ice Pack: Experiment, Data Analysis, and Modeling. IEEE Ocean. Eng. 43, 145-159, 2017
[6] F.B. Jensen et al. Computational Ocean Acoustics, Springer, 2011
[7] Kevin Heaney and Richard Campbell, “Effective ice model for under-ice propagation using the fluid-fluid parabolic equation”. Proceedings of Meetings on Acoustics, Vol. 19, 070052 (2013).
[8] E. K. Westwood , C. T. Tindle, and N. R. Chapman, “A normal mode model for acoustoelastic ocean environments,” J. Acoust. Soc. Am., 100, 3631-3645 (1996).
[9] M.D. Collins, “A split-step Padé solution for the parabolic equation method,” J. Acoust. Soc. Am. 93, pp. 1736-1742, 1993.